# LARGE-EDDY SIMULATION OF AN OSCILLATING-ROTATING TURBULENT FLOW

**Stefano Salon**, **Alessandro Crise**
Dipartimento di Oceanografia e di Geofisica Ambientale,
Istituto Nazionale di Oceanografia e di Geofisica Sperimentale-OGS
B.go Grotta Gigante 42/c, 34010 Sgonico, Trieste, ITALY
ssalon@inogs.it, acrise@inogs.it

**Vincenzo Armenio***
Dipartimento di Ingegneria Civile - Sez. Idraulica,
Universitá degli Studi di Trieste
34100 Trieste, Italy
armenio@dic.units.it

## ABSTRACT

In the present paper the effect of rotation over a turbulent Stokes boundary layer is investigated using large-eddy simulation. Both the vertical and the horizontal components of the rotation vector are considered in the equations governing the flow: this is a key point in the developing of Ekman boundary layers.
The main consequence of rotation is the breaking of the symmetry between the two half periods that characterizes the purely oscillating boundary layer. In agreement with relevant literature, this produces a stabilizing/destabilizing action over the turbulence activity. Turbulence appears enhanced compared to the purely oscillating case, especially during the second half cycle. Non-zero values of all Reynolds shear stresses in conjunction with the generation of a mean shear in the cross stream direction give rise to a larger production of turbulent kinetic energy. As a consequence, rotation increases the thickness of the turbulent boundary layer when compared to the case of the equivalent Stokes boundary layer. Finally, remarkable three-dimensionality is observed in the turbulent field.

## INTRODUCTION

The rotating and oscillating boundary layer (Ekman-Stokes BL) is prototypical to the study of the tidal flow in coastal areas. In the present work we discuss the results of a research designed to improve the knowledge of vertical turbulent mixing in shallow water basins.
It is well known that in nearly parallel flows the presence of a mean velocity shear normal to the axis of rotation may have either a stabilizing or a destabilizing effect, depending on whether the angular velocity and mean shear vorticity (i.e. the vorticity associated to the mean shear) have the same or opposite signs (see among the others Hopfinger and Linden, 1990; Kristoffersen and Andersson, 1993). The sign and the magnitude of the parameter $S$, defined as the ratio between the background vorticity and the mean shear vorticity, rule the importance of rotation in shear flows. In particular, the background vorticity and the shear vorticity are parallel if $S > 0$, and anti-parallel otherwise.
As pointed out by Kristoffersen and Andersson (1993), such vorticity ratio is a sort of a gradient rotation number. Following the intuition of Bradshaw (1969), who drove a formal algebraic analogy between the Richardson number and the parameters ruling the effect of rotation (or streamline curvature) on a turbulent flow, Tritton (1992) suggested to call $B = S(S + 1)$ (the equivalent gradient 'Richardson number' defined by Bradshaw, who first recognized its importance) the Bradshaw number. Since the Richardson number is negative for destabilized flow, the effect of rotation is therefore destabilizing when $B < 0$, that is when $-1 < S < 0$, and the maximum destabilization occurs for $B = -1/4$, that means $S = -1/2$. Both $S < -1$ and $S > 0$ are associated with stabilized flow. It is noteworthy that in turbulent shear flows 'stabilized' relates with decrease of turbulence intensity, and 'destabilized' relates with increase of turbulence intensity (Kristoffersen and Andersson, 1993).
The role played by $B$ in rotating flows was formally demonstrated by the experimental work of Johnston et al. (1972) by recasting the transport equations for the Reynolds stress tensor components, showing how the rotation may redistribute the energy among the components of the turbulent kinetic energy. The demonstration was reported by Coleman et al. (1990, henceforth referred to as CFS90) in their numerical study of the turbulent Ekman layer, which represents a stationary archetype of the neutral planetary boundary layer (PBL). In particular, CFS90 emphasized the significance of the source term $2\Omega_H(\langle w^2\rangle - \langle u^2\rangle)$, that is produced in the dynamic equation for the shear Reynolds stress $-\langle uw\rangle$ by the component of the Coriolis force associated with $\Omega_H$ ($w$ and $u$ are respectively the vertical and the streamwise components of the fluctuating velocity, $\Omega_H$ is the horizontal component of the Earth rotation, considered positive when parallel to the mean shear vorticity). Since the streamwise *rms* values are significantly larger than the vertical ones throughout the Ekman layer, a positive $\Omega_H$ implies a reduction, and a negative $\Omega_H$ means an increase of the turbulence activity, as known mainly related with $-\langle uw\rangle$. The role played by the background vorticity in the stability parameter $B$ is here expressed

*corresponding author

by $\Omega_H$, whereas the mean shear vorticity comes properly from the mean vertical gradient $dU/dz$. Since the oscillating flow changes periodically sign throughout the cycle, the associated vorticity will be parallel or anti-parallel to the background vorticity $\Omega_H$, and thus we expect that the flow will assume periodically stabilizing and destabilizing characteristics.
Due to the substantial influence played by the horizontal component $\Omega_H$ in turbulence activity, CFS90 concluded that the '$f$-plane' approximation cannot be adopted for numerical simulations of the Ekman layer. Similar conclusions were also previously drawn by Etling and Wippermann (1975) and Leibovich and Lele (1985).

The present paper deals with the analysis of the effects due to the recasting of a purely oscillating flow in a rotational frame, where the horizontal component of the rotation is perpendicular to the plane of the mean shear. The present work is a spin-off of a research project aimed at understanding the vertical turbulent mixing in critical conditions in the Gulf of Trieste, but can be intended to represent typical mid-latitude shallow water basins.

## THE PROBLEM FORMULATION

In large-eddy simulation the large scales of turbulence are directly resolved whereas the small-scale processes are parameterized by a subgrid-scale model. Such separation between scales is mathematically formalized by the filtering of the Navier-Stokes equations. The filtered, non-dimensional equations governing the rotating oscillating boundary layer driven by an harmonic pressure gradient aligned with the $x$-direction read as:

$$\frac{\partial \bar{u}_i}{\partial x_i} = 0, \tag{1}$$

$$\frac{\partial \bar{u}_i}{\partial t} + \frac{\partial \bar{u}_j \bar{u}_i}{\partial x_j} = -\frac{\partial \bar{p}}{\partial x_i} + \frac{1}{Re}\frac{\partial}{\partial x_j}\frac{\partial \bar{u}_i}{\partial x_j} + cos(t)\delta_{i1} + \frac{1}{Ro}\epsilon_{ijk}\hat{j}(sin(t)\delta_{k1} - \bar{u_k}) - \frac{\partial \tau_{ij}}{\partial x_j} \tag{2}$$

In eqs. 1 and 2, $\bar{\cdot}$ denotes the filtering operation. The coordinate $x_i$ (hereafter $x_1$, $x_2$, $x_3$ or $x$, $y$, $z$ are used interchangeably for the streamwise, spanwise and wall-normal directions) is made non-dimensional with the amplitude of motion $a = U_0/\omega$ (where $U_0$ is the amplitude of the velocity oscillation and $\omega$ is the angular velocity associated to the tidal flow), $t$ is the time coordinate made non-dimensional with $1/\omega$, $\bar{u_i}$ is the $i$-component of the filtered velocity field ($u_1$, $u_2$, $u_3$ or $u$, $v$, $w$ are used for the streamwise, spanwise and wall-normal velocity components) made non-dimensional with $U_0$, $\bar{p}$ is the filtered pressure field made non-dimensional with $\rho_0 {U_0}^2$, with $\rho_0$ the fluid density. The third term of the RHS is the non-dimensional, harmonic pressure gradient that drives the flow, and the fourth term is the non-dimensional Coriolis force associated with the oscillating inertial velocity proportional to $sin(t)$. The term $\tau_{ij}$ represents the subgrid-scale stresses that are parameterized by means of a dynamic-mixed model composed by an anisotropic scale-similar part (Bardina et al., 1980) and an eddy viscosity part (Smagorinsky, 1963). The Reynolds number $Re = aU_0/\nu$ is related to the amplitude of motion and the Rossby number $Ro = \omega/2\Omega$ is associated to the rotation $\Omega$. In the present work, we chose $Re = 1.6 \times 10^6$ that corresponds to a Stokes Reynolds number $Re_\delta = U_0\delta_S/\nu = 1790$ where $\delta_S = \sqrt{2\nu/\omega}$ is the nominal thickness of the Stokes BL and $\nu$ the kinematic viscosity. At this Reynold number the flow exhibits fully developed turbulence along most of the cycle (Salon et al., 2004a,b).
In our simulations, the frame of reference was designed in order to represent a tidal flow, driven by an oscillating pressure gradient, that is parallel to the SW-NE direction (towards NE in the first half of the cycle, towards SW in the second half). This configuration is related to the real features characterizing the site of the research project. The shear flow representing the tidal forcing has therefore a velocity $\langle u \rangle = \langle u(\bar{z}) \rangle$ aligned with the $x$-axis, whereas the rotation vector $\mathbf{\Omega}$ has the horizontal component $\Omega_H$ parallel to the northward direction and the vertical component $\Omega_V$ normal to the $xy$ plane. Considering $\Omega_H = (\Omega_x, \Omega_y)$, each rotated by $45^o$ with respect to $\Omega_H$, the angular velocity, that defines the Coriolis term in the RHS, has thus the following components: $\mathbf{\Omega} = (\Omega_x, \Omega_y, \Omega_z) = \Omega(1/2, 1/2, 1/\sqrt{2}) = f(1/2\sqrt{2}, 1/2\sqrt{2}, 1/2)$. Therefore, the parameter $S$ reads as: $S = 2\Omega_y/\zeta$, where $\zeta = dU/dz$ is the mean shear vorticity. The Rossby number $Ro$ can be expressed as the ratio between the inertial and the rotational angular velocities: in the present simulation it can be expressed as $Ro = \omega_{M2}/f = 1.4$, where $\omega_{M2}$ is the angular velocity associated to the M2 component of the tidal flow (period of 12.4206 hours) and $f = 2\Omega sin\phi$ is the Coriolis parameter that has a value typical for the mid-latitudes ($\phi = 45^o$). The Coriolis force introduces a transverse pressure gradient in the cross-stream component of the momentum equation, thus originating an oscillation also in the cross-stream velocity component.
Following CFS90, the turbulent Ekman layer is characterized by a Reynolds number dependent on the intensity of the geostrophic wind speed: $Re_G = G/\sqrt{\nu f/2}$. In our case the role of the geostrophic flow is played by the tidal forcing, $G = U_0$. We obtain $Re_G \approx 2100$, which is as large as four times than the higher Reynolds number investigated by CFS90.
Previous numerical studies (DNS by Kristoffersen and Andersson, 1993, and LES by Tafti and Vanka, 1991) investigated turbulent channel flow at low Reynolds numbers and at different rotation rates, being particularly interested in relaminarization effects and in rotational-induced structures. As previously stated, our interest is instead more focused on the influence of rotation in a periodically driven turbulent flow.

The numerical model solving the equations was developed by Armenio and Piomelli (2000). A no-slip boundary condition is imposed at the bottom wall, a free-slip condition is adopted at the top boundary, and due to the homogeneous character of turbulence in the streamwise and spanwise directions, periodic boundary conditions are employed. The initial condition is represented by a turbulent state relative to a $0^o$-phase of the purely oscillating case. The data of the first two cycles of oscillation were not used for the evaluation of the statistics, since they are affected by an initial transient due to the introduction of the rotation in the purely oscillating field. The statistics were accumulated averaging over the $xy$ planes of homogeneity, and in phase over the whole cycle.
The computational grid has $64 \times 128 \times 256$ points, respectively in the streamwise, spanwise and wall-normal directions. The dimensions of the box were chosen in order to guarantee that it has an adequate resolution of the large-scale energy-carrying turbulent structures: following Salon et al. (2004a), we chose $L_x = L_y \approx 50\delta_S$ and $L_z \approx 40\delta_S$, where $\delta_S$ is the Stokes layer

thickness previously defined. This choice gives $\Delta x^+ \approx 70$, $\Delta y^+ \approx 20$ and $\Delta z^+$ spanning between 2 and 22, based on the maximum value of the friction velocity along the cycle.

## RESULTS AND DISCUSSION

Figure 1 shows results of the rotating-oscillating flow, in comparison with the same quantities computed for the purely oscillating flow with the same grid resolution. In particular, we plot temporal evolutions of the streamwise and the spanwise velocities, $\bar{u}$ and $\bar{v}$, as recorded at the free-surface ($\bar{v}$ is obviously zero in the purely oscillating flow), the wall shear stress $\tau_w$ and the resolved, specific turbulent kinetic energy defined as

$$E = \frac{1}{V} \int (u''^2 + v''^2 + w''^2)\, dV$$

where $V = L_x L_y L_z$ is the volume of the computational box and the symbol $''$ denotes fluctuating resolved quantities (hereafter with $'$ we indicate the total fluctuating quantity, namely resolved + SGS contribution).

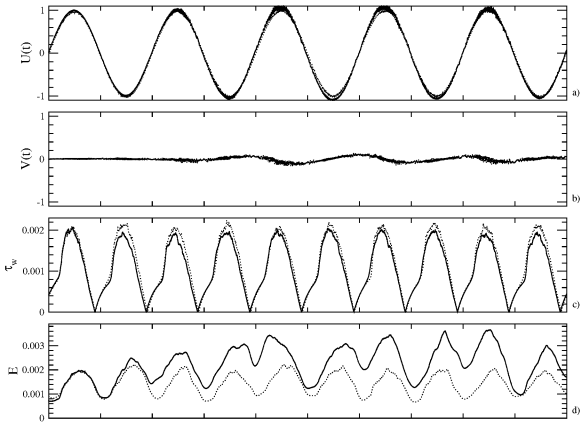


Figure 1: Evolution along the first five periods of simulation of relevant bulk quantities (solid line) and comparison with the turbulent Stokes BL (dotted line): a) free-surface streamwise velocity; b) free-surface spanwise velocity; c) wall shear stress; d) specific turbulent kinetic energy.

Due to the additional Coriolis terms in the equations, the streamwise velocity (Fig. 1a) appears slightly larger than that of the purely oscillating case in those phases when the largest values of the spanwise component occur, in particular during the first half period. Such increase can be explained if we consider a feedback mechanism between the horizontal components of the velocity, which develops consequently to the introduction of rotation in the system. The initial, very small values of the cross-stream velocity induced by the rotation grow as long as the simulation goes further (up to reach a stationary situation) and increase the magnitude of the Coriolis term present in the momentum equation, and therefore the streamwise velocity, which in turn influences the cross-stream component (Fig. 1b). Similarly to the laminar flow (not discussed here), the free-surface cross-stream component is about one order of magnitude smaller, and it has a phase-lag with respect to the streamwise one: this means that a Lagrangian particle buoying over the surface will experience an elliptic path whose minor axis is about one tenth of the major one.
The wall shear stress (Fig. 1c) appears to be about 5% smaller than that of the purely oscillating case, and its maximum value gives a friction coefficient $f_w \simeq 0.004$, which is very close to that obtained in the purely oscillating flow. Such similarity can be explained by the fact that, as well known, the work done by the Coriolis force on the flow is zero, and no additional viscous stresses are produced by a constant rotation (Tritton, 1988). The value of $u_\tau$ associated to the maximum wall shear stress is in good agreement with what expected, for a value of $Re_G \approx 2100$, by the extrapolation at higher Reynolds number described by CFS90 (see Fig.22a).
The temporal evolution of the turbulent kinetic energy resembles that recorded in the purely oscillating case, characterized by phases where turbulence tends to switch off. However, the energetic peaks are more than one third larger than the oscillating case: this is an effect of the Coriolis force that, besides rising a cross-stream velocity, generates additional terms in the transport equation of the turbulent kinetic energy, as shown in a next section. On the other hand, the total kinetic energy (not shown) correctly does not change with respect to the non-rotating case.

### Mean velocity fields

The mean vertical profiles of the streamwise velocity made non-dimensional with $U_0$ (Fig. 2) are plotted every $15^o$ only for the first half cycle. The rotation slightly affects the second half of the cycle (from $180^o$ to $360^o$), corresponding to a tidal current flowing from NE to SW: the relative magnitude of the mean profiles is about 1% larger than that of the first half, in particular for $z_d > 20\delta_S$ and phases between $150^o$ and $180^o$. The profiles differ from those of the purely oscillating case in the central phases, between $75^o$ and $150^o$ (Fig. 2b,c,d). The differences are more evident in the layer $2\delta_S \lesssim z_d \lesssim 30\delta_S$ and are due to the presence of the cross-stream velocity. It is noteworthy that the bulge which characterizes both the laminar (Tritton, 1988) and the turbulent Ekman layer (CFS90), and also the turbulent Stokes BL (Salon et al., 2004a,b) is here practically absent. This has to be ascribed to the combined effect of oscillation and rotation and is related to an additional increase of the Reynolds shear stresses with respect to the molecular ones.

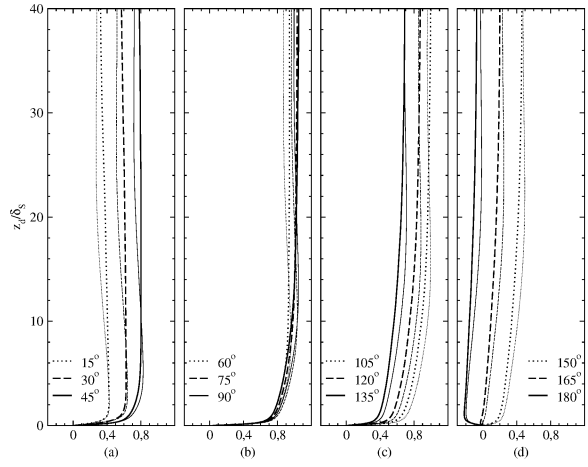


Figure 2: Non-dimensional mean streamwise velocity $\langle u \rangle / U_0$ for the rotating-oscillating flow (thick lines) and for the purely oscillating flow (thin lines).

The mean vertical profiles of the cross-stream velocity

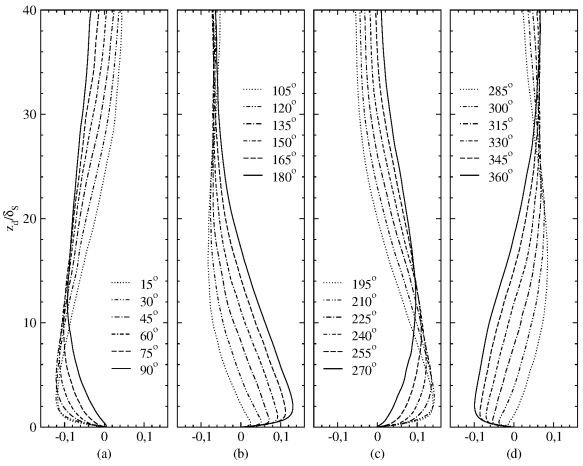


Figure 3: Non-dimensional mean spanwise velocity $\langle v \rangle / U_0$.

(Fig. 3), significantly differ during the two parts of the cycle. Similarly to what observed in the laminar case, the profiles evolve throughout the cycle and the vertical location where the maximum value of velocity occurs varies along the cycle.. The associated near-wall layer, evaluated as the distance from the maximum of $\langle v \rangle$ to the wall, is very thin and close to the wall at $90^o$ (end of the first accelerating phase, Fig. 3a) and increases up to $z_d \approx 14\delta_S$ between $270^o$ (Fig. 3c) and $285^o$ (Fig. 3d, end of the second accelerating phase), then it is again very close to the wall. The maximum value reads about $-0.13$ at $30^o$ and about 0.14 at $210^o$, both at $z_d \approx 3\delta_S$, which is of the same order of that evaluated by CFS90.
Due to the oscillation, the turbulent depth $\delta_T$ defined by CFS90 as the ratio between the friction velocity and the Coriolis parameter, evolves in our case throughout the cycle, being on average maximum at $75^o$ (and $255^o$) and zero at $160^o$ (and $340^o$). The maximum value is $\delta_T = u_\tau / f = 54\delta_S$, which due to the choice of the computational domain, is more than one third larger than $L_z$. For a Reynolds number equal to 400, CFS90 estimated an Ekman layer height (defined where $\langle v \rangle = 0$) of about $0.7\delta_T$: the same relation with $\delta_T$ gives in our case an Ekman layer height as high as $z_d \approx 38\delta_S$, that corresponds to $\langle v \rangle = 0.07$. This explains the presence of an elliptic trajectory at the surface, which, on the other hand, is also observed in the full-scale case, and also of the non-zero values of the spanwise velocity at the top of the domain. Note that in the purely oscillating case the depth of the turbulent layer amounts to about $25\delta_S$.

The mean spanwise velocity shows a phase-lag decreasing going further from the wall: the axes of the corresponding elliptic paths (Fig. 4) therefore rotate clockwise moving from the surface down to $z_d = 10\delta_S$, they do not change at $z_d = 6\delta_S$ and then reverse the sense of rotation down to the wall. The minor axis is maximum at $z_d = 2\delta_S$, as also shown in Fig. 3. Thus, the combined effect of oscillation and rotation and the depth-dependent phase-lag between the horizontal velocity components prevents from the formation of the "Ekman spiral" in the present flow.

#### Reynolds stresses

Rotation induces a non-zero cross-stream velocity, thus the Reynolds shear stresses associated to $v'$, namely $\tau_{12} = \langle u'v' \rangle$ and $\tau_{23} = \langle v'w' \rangle$, are no longer zero as in the purely oscillating flow, and they are not negligible when compared to $\tau_{13} = \langle u'w' \rangle$.

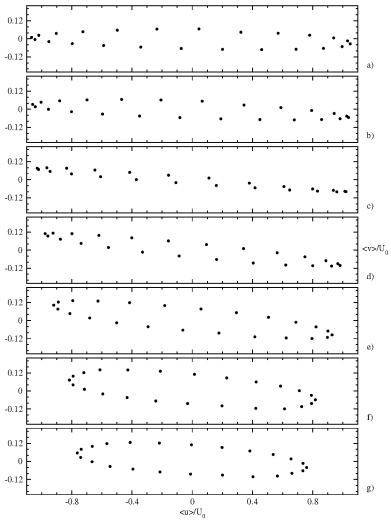


Figure 4: Elliptic paths: mean spanwise *vs* mean streamwise velocity at different planes : a) $z_d = 40\delta_S$; b) $z_d = 30\delta_S$; c) $z_d = 20\delta_S$; d) $z_d = 10\delta_S$; e) $z_d = 6\delta_S$; f) $z_d = 2\delta_S$; g) $z_d = \delta_S$. The axis ratio is 1 : 5.

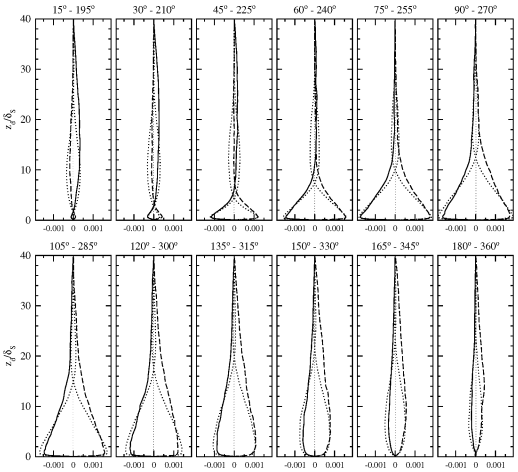


Figure 5: Non-dimensional mean Reynolds shear stress $\langle u'w' \rangle / U_0^2$ for the rotating-oscillating flow from $15^o$ to $180^o$ (solid line), from $195^o$ to $360^o$ (dashed line) and for the purely oscillating flow (dotted line).

Figure 5 shows the vertical profiles of the non-dimensional Reynolds shear stress $\langle u'w' \rangle$ plotted every $15^o$ throughout the whole cycle, from the wall to the surface. The beginning of the turbulence activity is observable during the accelerating phases of the two half periods, respectively at $45^o$ and at $225^o$. Turbulence appears well sustained during the central phases (from $60^o$ to $135^o$ and from $240^o$ to $315^o$) and near the wall, with intensity comparable to the purely oscillating case at $z_d < 10\delta_S$, and larger for $z_d > 10\delta_S$. A remarkable difference from the purely oscillating flow is the absence of the sign change of $\langle u'w' \rangle$ in most of the cycle (from $75^o$ to $165^o$ during the first half-period and from $225^o$ to $345^o$ during the second). This is associated to the behavior of the mean verti-

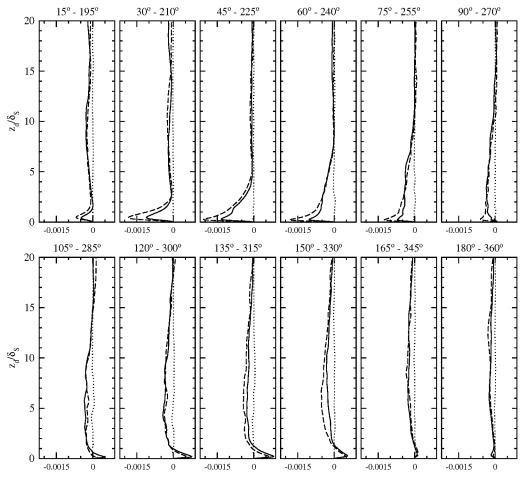


Figure 6: Non-dimensional mean Reynolds shear stress $\langle u'v' \rangle / U_0^2$ for the rotating-oscillating flow from $15^o$ to $180^o$ (solid line), from $195^o$ to $360^o$ (dashed line) and for the purely oscillating flow (dotted line).

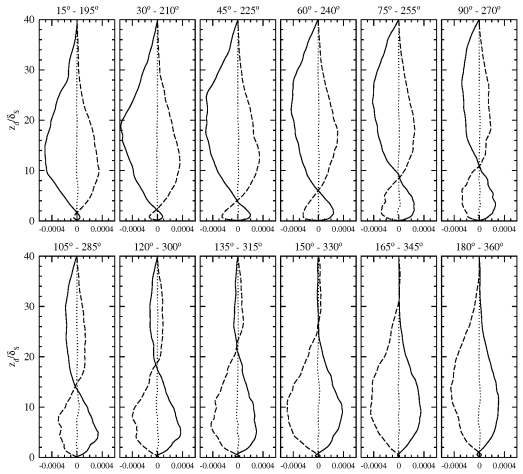


Figure 7: Non-dimensional mean Reynolds shear stress $\langle v'w' \rangle / U_0^2$ for the rotating-oscillating flow from $15^o$ to $180^o$ (solid line), from $195^o$ to $360^o$ (dashed line) and for the purely oscillating flow (dotted line).

cal shear $d\langle u \rangle / dz$ (see Fig. 2) which holds its sign during most of the cycle, and, as a consequence, to the absence of the bulge in the mean streamwise velocity profile. Unlike the oscillating flow, non-zero values of $\tau_{13}$ are present in the outer layer, at $z_d > 20\delta_S$, and larger intensities characterize the second half-period, corresponding to tidal current moving from NE to SW. From $255^o$ to $315^o$ $\tau_{13}$ is on average as high as 34% than $\tau_{13}$ from $75^o$ to $135^o$, and the difference increases up to 93% at the phase $345^o$ with respect to $165^o$. The anticipated stabilizing/destabilizing effect of rotation on turbulence activity is therefore here observable. In particular, we recognize the *east/west enhancement/reduction trend* stated by CFS90: when the tidal forcing flows from SW to NE (from NE to SW), corresponding to the first (second) half-period, it produces a mean vorticity which is parallel (anti-parallel) with $\Omega_H$ and thus stabilizes (destabilizes) the turbulent activity.

The fluctuations of the horizontal velocity components (Fig. 6) appear strongly correlated only near the wall, for

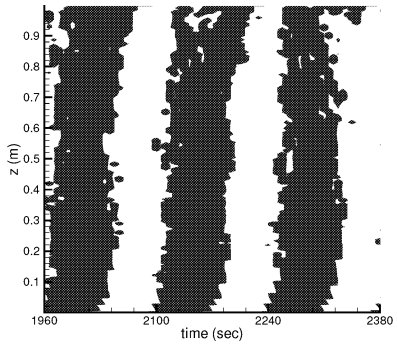


Figure 8: Bradshaw number $B$ for three cycles of simulation (period is 140 s): shading represents positive values of $B$.

$z_d < 5\delta_S$, exactly where the mean cross-stream velocity achieves the maximum amplitudes. The correlation is also larger in the second half-period of oscillation, between $30^o$ and $75^o$, when a rapid increase of the turbulence activity is observed, and the maximum value at $45^o$ is comparable with the maximum of $\tau_{13}$ at $90/270^o$. Negative, larger values of $\tau_{12}$ characterize the accelerating phases, while the decelerating ones (from $105/285^o$ to $165/345^o$) experience positive and smaller values.

The cross-stream and the vertical velocity fluctuations are correlated (Fig. 7) along the whole column and throughout the whole cycle of oscillation, with intensities that are around one third of the largest magnitudes of $\tau_{13}$. In particular the height which corresponds to the reverse point (where the sign of $\tau_{23}$ changes) of the first half-period coincides with that of the second half-period for all the phases. The reverse point evolves during the phases, going away from the wall up to $z_d \approx 22-26\delta_S$ between $135/315^o$ and $150/330^o$, when another reverse point develops very close to the wall. An asymmetry between the two half-periods, already observed for $\tau_{13}$, can be observed in the outer layer, near the surface: in this case the turbulence activity involving $v$ and $w$ is more intense with forcing coming from SW during the first accelerating phases, near the surface, whereas in the last decelerating phases the usual "east enhancement" is observable in the lower half of the column.

A complementary analysis of the three components of the Reynolds stress suggests that a turbulent state is always present throughout the cycle. Although $\tau_{13}$ is significant (larger than $0.001U_o^2$) from $45/225^o$ to $120/300^o$, $\tau_{12}$ is stronger near the wall between $30/195^o$ and $60/240^o$ and $\tau_{23}$ has values order $0.0005U_0^2$ in the outer layer from $150/330^o$ to $45/225^o$, but is always non-zero during the cycle, in particular far from the wall. The structure of turbulence appears to be completely three-dimensional, with a well established anisotropic behavior.

In order to have a further confirm of the agreement of our results with theory, we plot in Figure 8 the value of the Bradshaw number $B$ as previously defined: the sign of $B$ is positive (negative) for stable (unstable) conditions corresponding to tidal forcing current coming from SW (NE).

A comparative analysis of the three turbulence intensities (not shown here) indicates that although the streamwise component is only slightly affected by the rotation, the vertical

and the cross-stream components appear considerably influenced by rotation, in particular far from the wall, even if the temporal evolution does not remarkably change with respect to the non-rotating case.
Stable conditions, corresponding to tidal current coming from SW, increase cross-stream turbulence intensity especially near the surface and during the accelerating phases, while unstable conditions affect turbulence, although at a minor extent, in particular in the late decelerating phases. In the outer layer and near the top of the computational domain, tidal forcing from SW affects the vertical fluctuations in particular during the accelerating phases, producing intensities larger than those observed in the purely oscillating case.
The result of the present study are consistent with those of CFS90, although the latter are relative to different flow and boundary conditions. Specifically, as in CFS90, we observe a near-surface behavior characterized by small but non-zero horizontal fluctuations. Moreover, CFS90 addressed to a *streamwise-spanwise reversal* which in our simulation is observable near the surface, during the central phases of the unstable half-period, when spanwise fluctuations result larger than their streamwise counterparts.

## CONCLUSIONS

The rotating-oscillating boundary layer is investigated in the present paper. To the best of our knowledge this is the first numerical study of such a turbulent flow field.

Recasting of a purely oscillating flow in a rotational frame has the main effect of breaking the symmetry between the two half cycles of the oscillation period.
Moreover, rotation has a twofold effect on the system dynamics: in the first half cycle, corresponding to forcing from SW to NE, the mean vorticity (related to the mean vertical shear) is parallel to the background vorticity and consequently turbulence tends to be stabilized and its activity decreases; conversely, in the second half period, where forcing goes from NE to SW, the mean vorticity is opposite to the background one and thus turbulence tends to be destabilized and its activity increases. Therefore, as shown in Fig.5, turbulence activity increases when compared to the pure oscillating case, in particular in the bottom half of the water column and during the decelerating phases of the cycle (from $90^o$ to $165^o$ and from $270^o$ to $360^o$), being always more intense in the second half period. Such a stabilizing/destabilizing effect agrees with theory, as described in Hopfinger and Linden (1990) and CFS90, and emphasizes the importance played by the horizontal component of the Earth rotation vector in the dynamics of turbulent Ekman layers.
Our results show non-zero correlations between horizontal velocity fluctuations ($\tau_{12}$) and between spanwise and vertical components ($\tau_{23}$), and also an increase of the vertical and cross-stream turbulence intensities when compared to the purely oscillating flow. This picture describes thus a highly three-dimensional character of turbulence, affecting the three spatial directions. The evolution of $B$ throughout the cycle is also correctly reproduced (Fig.8), together with the enhancement trend of turbulence observed with inertial forcing coming from eastern quarters of the compass, as also addressed by CFS90.
The horizontal and vertical mixing appears therefore to be enhanced by the rotation, and especially when tidal current flows from NE. Differently from what observed in the purely oscillating case, turbulence activity spans over the three directions, with stronger intensity along the horizontal planes near the wall during the first accelerating phases. Rotation also produces the thickening of the depth of fluid where developed turbulence is observable.

## ACKNOWLEDGMENTS

This research was financially supported by the Istituto Nazionale di Oceanografia e di Geofisica Sperimentale - OGS of Trieste (Italy), under the contract "Modellistica integrata dei fenomeni di trasporto e trasformazione biologica della materia".

## REFERENCES

Armenio, V. and Piomelli, U., 2000, "A Lagrangian mixed subgrid-scale model in generalized coordinates", *Flow Turbulence and Combustion*, Vol. 65, 51.

Bardina, J., Ferziger, J. H. and Reynolds, W. C., 1980, "Improved subgrid scale models for large eddy simulation", *AIAA paper* No.80-1357.

Bradshaw, P., 1969, "The analogy between streamline curvature and buoyancy in turbulent shear flow", *J. Fluid Mech.*, Vol. 36, 177.

Coleman, G. N., Ferziger, J. H. and Spalart, P. R., 1990, "A numerical study of the turbulent Ekman layer", *J. Fluid Mech.*, Vol. 213, 313.

Etling, D. and Wippermann, F., 1975, "On the stability of a planetary boundary layer with Rossby number similarity", *Boundary-layer Met.*, Vol. 9, 341.

Hopfinger, E. J. and Linden, P. F., 1990, "The effect of background rotation on fluid motions: a report on Euromech 245", *J. Fluid Mech.*, Vol. 211, 417.

Johnston, J. P., Halleen, R. M. and Lezius, D. K., 1972, "Effects of spanwise rotation on the structure of two-dimensional fully developed turbulent channel flow", *J. Fluid Mech.*, Vol. 56, 533.

Kristoffersen, R. and Andersson, H. I., 1993, "Direct simulations of low-Reynolds-number turbulent flow in a rotating channel", *J. Fluid Mech.*, Vol. 256, 163.

Leibovich, S. and Lele, S. K., 1985, "The influence of the horizontal component of Earth's angular velocity on the instability of the Ekman layer", *J. Fluid Mech.*, Vol. 150, 41.

Salon, S., Armenio, V. and Crise, A., 2004a, "A numerical investigation of the Stokes boundary layer in the turbulent regime", *submitted to J. Fluid Mech.*.

Salon, S., Armenio, V. and Crise, A., 2004b, "Studio numerico dello strato limite di Stokes in regime turbolento", *Proceedings, XXIX Convegno Nazionale di Idraulica e Costruzioni Idrauliche*, Ed. Bios, Vol. 1, 291.

Smagorinsky, J., 1963, "General circulation experiments with the primitive equations. I. The basic experiment", *Mon. Weath. Rev.*, Vol. 91, 99.

Tafti, D. K. and Vanka, S. P., 1991, "A numerical study of the effects of spanwise rotation on turbulent channel flow", *Phys. Fluids*, Vol. 3, 642.

Tritton, D. J., 1988, *Physical Fluid Dynamics*, Oxford University Press Inc., New York, 519 pp.

Tritton, D. J., 1992. "Stabilization and destabilization of turbulent shear flow in a rotating fluid", *J. Fluid Mech.*, Vol. 241, 503.